

Article

Calibration of Model Parameters for Soda Saline Soil-Subsoiling Component Interaction Based on DEM

Min Liu ¹, Jingli Wang ¹, Weizhi Feng ¹, Haiyang Jing ¹, Yang Wang ², Yingjie Guo ¹ and Tianyue Xu ^{1,*}

¹ College of Engineering and Technology, Jilin Agricultural University, Changchun 130118, China; liumin9711@163.com (M.L.); wjlwy2004@sina.com (J.W.); fengweizhi@jlu.edu.cn (W.F.); jinghy0110@163.com (H.J.); 13944097153@163.com (Y.G.)

² College of Biological and Agricultural Engineering, Jilin University, Changchun 130021, China; yangw12@mails.jlu.edu.cn

* Correspondence: ellen1116@126.com

Abstract: To apply the discrete element method (DEM) to simulate the interaction process between soda saline–alkali soil and subsoiling component in Northeast China, establishing the soda saline–alkali soil particle model and selecting more accurate simulation parameters are important. In this paper, we studied the soda saline–alkali soil of the Songnen Plain in China. First, we studied the geometric shape of soda saline–alkali soil particles and proposed a modeling method for single soil particles based on the multisphere combination method. Considering the cohesion of soda saline–alkali soil particles, the Hertz–Mindlin with JKR (JKR) model was used as the contact model between soil particles. Then, the calibration method was used to obtain simulation parameters of soils that are difficult to obtain experimentally. We conducted soil angle of repose (AoR) tests, the Plackett–Burman (PB) tests, and steepest ascent (SA) tests in turn to perform a sensitivity analysis for microscopic contact parameters and select the parameters that have a significant effect on the response value (static AoR), i.e., soil surface energy, soil–soil static friction coefficient, and soil–soil rolling friction coefficient. Then, the optimal combination of simulation parameters was obtained via the Box–Behnken (BB) tests, using ANOVA to optimize the multiple regression equation. Finally, the optimal parameter combination was verified by the AoR test and the direct shear (DS) test. The results showed that the parameters had good adaptability for the AoR test. However, the simulation results of the DS test were significantly different from the experimental values. Therefore, the contact model needs to be further modified by adding Bonding bonds between soil particles based on the JKR model and further correcting for Rayleigh time step, shear modulus, and surface energy. By comparing the simulation and the experimental results, it was found that the simulation results obtained from both the DS test and AoR test had relatively small errors relative to physical tests, the two trends are the same, and the values are similar. This verified the feasibility and effectiveness of the soda saline–alkali soil particle modeling method and parameter selection proposed in this paper.



Citation: Liu, M.; Wang, J.; Feng, W.; Jing, H.; Wang, Y.; Guo, Y.; Xu, T. Calibration of Model Parameters for Soda Saline Soil-Subsoiling Component Interaction Based on DEM. *Appl. Sci.* **2023**, *13*, 11596. <https://doi.org/10.3390/app132011596>

Academic Editor: Nathan J. Moore

Received: 26 September 2023

Revised: 20 October 2023

Accepted: 20 October 2023

Published: 23 October 2023

Keywords: soda saline–alkali soil; contact model; parameter selection; DEM



Copyright: © 2023 by the authors. Licensee MDPI, Basel, Switzerland. This article is an open access article distributed under the terms and conditions of the Creative Commons Attribution (CC BY) license (<https://creativecommons.org/licenses/by/4.0/>).

1. Introduction

The Songnen Plain in Northeastern China, is home to one of the world's three major concentrations of soda saline–alkali soil. Recently, soil saline–alkali desertification is on the rise. Subsoiling technology is widely recognized as an effective engineering solution for improving saline lands. To develop an optimal subsoiling component for soda–saline land improvement, we utilized DEM for simulation. Given the inherent contact between subsoiling components and soil particles during the subsoiling process, it is crucial to establish a more accurate model of soda saline–alkali soil particles when using the DEM [1–4] to analyze these contact effects and optimize the design of related mechanical components [5,6].

Soil exhibits pronounced anisotropic and nonlinear behavior, characterized by a complex constitutive relationship. Its properties are profoundly influenced by factors such as water and organic matter content, porosity, and texture. A comprehensive review of the literature underscores the abundance of research dedicated to the physicochemical properties of soda saline–alkali soils [7–12], yet investigations into their physical and mechanical properties are notably scarce. Given the unique physicochemical attributes of soda saline–alkali soil, distinct from those of typical soil, further exploration into how these properties influence physical and mechanical characteristics is imperative. The discrete element method (DEM) is a numerical method for analyzing and solving the dynamic problems of complex discrete systems. It is widely used in the simulation of particle structures [13]. The discrete element method can integrate the contact mechanics model of soil particles to simulate the microscopic and macroscopic deformation of particles and the interaction between soil particles and machinery [14]. Because the micro-contact parameters between soil particles cannot be directly measured by experiments, they need to be obtained through repeated simulation experiments. When utilizing the Discrete Element Method (DEM) to simulate and analyze the movement of soil particle assemblies, it is necessary to calibrate the contact parameters of soil particles such as restitution coefficient, static friction coefficient, and rolling friction coefficient [15].

Many scholars have studied the calibration of soil particle contact parameters using different contact models. The JKR model is suitable for the simulation between wet materials and easily bonded particles, and the cohesion in the model can better characterize the bonding characteristics of soil particles. Zhu, Li, Xing, Hao, et al. used a JKR contact model to calibrate the contact parameters between soil particles with the angle of repose as the response value [16–19]. The Hertz–Mindlin with Bonding (HMB) model binds two particles together by “bond”, which can characterize the cohesion between soils. Du et al. used HMB and JKR contact models to conduct comparative tests, combined with soil bin test results, to study the mixing performance of rotary tillers and spiral horizontal blade rotary tillers in silty clay loam [20]. Hang et al. used the HMB contact model to establish a layered soil model to study the soil disturbance during the subsoiling process [21].

Within DEM analyses, soil particles are conventionally defined as spheres due to the computational simplicity of calculating contacts between spherical particles, as it enhances the simulation efficiency [22]. Song, Li, et al. defined soil particles using a single-sphere model and established a soil bin model to analyze soil disturbance during tillage [23]. However, the real-world size and shape of soil particles are inherently more intricate; the relationship between the macroscopic and microscopic characteristics of soil particle groups has yet to be fully understood [24,25]. The equal diameter soil particles cannot fully reflect the influence of the particle size distribution of the actual soil on the interaction between the soil particles and the working parts [26]. It is imperative to recognize that spherical particles alone cannot adequately characterize the accurate shape of soil particles. Song et al. calibrated and optimized the bonding parameters between soil particles by taking the non-equal-diameter soil particles in a mulberry field as the research object. [27]. Zhang et al. established four soil particle models with different sizes and shapes for simulation and verified the accuracy of the simulation model [28].

At present, there are few studies on the particles and particle aggregates of soda saline–alkali soil in Northeast China. When DEM is used for a simulation, the contact parameters between the soil particles are worth studying; the meticulous verification of the accuracy of the model also demands thorough analysis and consideration. In this study, we used DEM to calibrate soil particle contact parameters in soda saline soils of the Songnen Plain, Northeast China, using the angle of repose as the response value. To verify the accuracy of the calibration parameters, we conducted the DS test and added the bond between soil particles based on the JKR model to accurately simulate the soil bonding characteristics. Finally, the contact model and contact parameter combination of soil particles were determined, which provided a theoretical basis for the subsequent development of subsoiling machinery in soda saline–alkali land in Northeast China.

2. Materials and Methods

This paper comprehensively examined and analyzed soda saline–alkali soil, encompassing particle shape, size distribution, and physical and mechanical properties. Recognizing the adhesion characteristics of soil, we employed the Hertz–Mindlin with JKR (JKR) model as the contact model. First, using soil angle of repose (AoR) tests, we conducted the Plackett–Burman (PB), steepest ascent (SA), and Box–Behnken (BB) tests sequentially to select and calibrate the sensitive parameters in the model. Second, we obtained the optimal parameter combination by variance analysis. Finally, to improve the reliability of the verification, two different tests were used to verify the calibrated parameter combination, that is, the AoR test and direct shear (DS) test. Considering the adhesion characteristics of saline–alkali soil and the characteristics of high firmness and easy hardening, bonds are added between soil particles based on the JKR model. Combined with the physical test and simulation results, the contact model and sensitivity parameters are further corrected, in order to provide a reference for the discrete element simulation parameters of soda saline–alkali soil and subsoiling machine in Northeast China.

The soda saline–alkali soil samples were collected on 12 May 2022, at an outdoor temperature of 21 °C. The collection site, situated in Sanye Village, Haituo Township, Daan City, Jilin Province (123.96° E; 45.32° N), is centrally located within the Songnen Plain (see Figure 1). This area is characterized by a temperate semi-humid and semi-arid climate, typical of a continental climate. The soil in this region exhibits an average pH value of 9.5 and an average total salt content of 0.7%, which is heavily salinized soil that has not been cultivated and reclaimed, representing the original landform characteristics of soda saline land under native conditions, as shown in Figure 2.



Figure 1. Administrative map of Daan City.



Figure 2. Saline landform pictures.

To comprehensively consider the water and salt transport characteristics within soda saline–alkali soil, three sampling plots were randomly selected, and we employed the five-point sampling method. Using a shovel, soil samples were obtained at depths of 0–10 cm, 10–20 cm, 20–30 cm, and 30–40 cm below the surface [29]. Each collected soil sample was placed in a self-sealing bag, meticulously numbered for identification purposes, and its wet weight was measured on-site. This process was replicated for a total of 20 samples within each land block.

2.1. Soda Saline–Alkali Soil Particle Size and pH Value Test

Soil particle size analysis was conducted using the screening method, which determined the percentage of each particle group within the overall mass of soil particles. To ensure the precise determination of soil pH, we entrusted the soil to a specialized testing agency. Soil pH measurements were performed using the PHSJ-6L pH meter, provided by Shanghai Yidian Scientific Instrument Co., Ltd. (Shanghai, China).

2.2. Water Content, Density, and Firmness Test of Soda Saline–Alkali Soil

Moisture content analysis was conducted using the drying method. Soil samples were placed in aluminum boxes, and the drying oven was set to a temperature of 105 °C. The soda saline–alkali soil-filled aluminum boxes were dried for a period of 8 h until a constant weight was achieved. The weight lost during this process represented the quantity of water contained within the sample.

Soil samples were obtained using a ring knife with a volume of $V = 100 \text{ cm}^3$. The ring knife, containing the soil sample, was then weighed using an electronic balance. This procedure was repeated three times for each sample, and the average value was calculated as the density of soda saline–alkali soil.

The TYD-2 hardness tester, manufactured by Zhejiang Top Instrument Co., Ltd. (Hangzhou, China), was vertically inserted into the soil. Soil firmness measurements for the 0–40 cm soil layer were obtained by recording the readings.

2.3. Simulation Contact Model

Considering the distinctive attributes of soda saline–alkali soil in Northeast China, characterized by the soil's propensity for bonding and elevated water content, we opted for the JKR model, which is particularly well-suited for small particles and materials exhibiting wet bonding properties, in our simulation analysis. Within the JKR model, the calculation of tangential contact force, normal damping force, and tangential damping force closely parallels that of the Hertz–Mindlin (no-slip) (HM) contact model. Within the JKR model, the tangential contact force, normal damping force, and tangential damping force are calculated similarly to the Hertz–Mindlin (no-slip) (HM) contact model, and the cohesive force explains the normal contact force in the JKR theory [30,31]. In this paper, the macroscopic bonding characteristics between soil particles are explained by surface energy, and the contact force between particles can be expressed as follows:

$$F_{JKR} = \frac{4E^*}{3R^*}\alpha^3 - 4\sqrt{\pi\Delta\gamma E^*}\alpha^3 \quad (1)$$

$$\delta_n = \frac{\alpha^2}{R^*} - \sqrt{\frac{4\pi\gamma\alpha}{E^*}} \quad (2)$$

$$F_t^c = K_t\delta_t \quad (3)$$

$$F_n^d = 2\sqrt{\frac{5}{6}}\beta\sqrt{K_n m^* v_n} \quad (4)$$

$$F_t^d = 2\sqrt{\frac{5}{6}}\beta\sqrt{K_t m^* v_t} \quad (5)$$

where F_{JKR} is the JKR normal contact force, N; F_t^c , F_n^d , and F_t^d are the tangential contact force, normal damping force, and tangential damping force, N; δ_n is the normal overlap of particles, m; δ_t is the tangential overlap of particles, m; α is the contact radius of particles, m; γ is the surface energy, N/m; v_n and v_t are the normal and tangential components of the relative velocity of particles, m/s; E^* is the equivalent elastic modulus, Pa; and R^* is

the equivalent contact radius, m . The equivalent elastic modulus, E^* , and the equivalent contact radius, R^* , are defined as shown in Equations (6) and (7).

$$\frac{1}{E^*} = \frac{1 - \nu^2}{E_1} + \frac{1 - \nu^2}{E_2} \quad (6)$$

$$\frac{1}{R^*} = \frac{1}{R_1} + \frac{1}{R_2} \quad (7)$$

In the equation, E_1 and E_2 are the elastic moduli of particles 1 and 2, Pa; ν_1 and ν_2 are Poisson's ratios of particles 1 and 2; and R_1 and R_2 are the contact radii of particles 1 and 2, m.

2.4. Soil Particle Simulation Model

Since the soda saline–alkali soil in the Songnen Plain of Northeast China has high cohesiveness when the water content is 18%, the soil particles will be bonded into agglomerates. Our observation of the agglomerates formed by soil particles revealed that most of them showed shapes similar to spheres, ellipsoids, and cones, as shown in Figure 3. Consequently, the geometric model for soil particles can be constructed based on these three fundamental shapes, as illustrated in Figure 4.

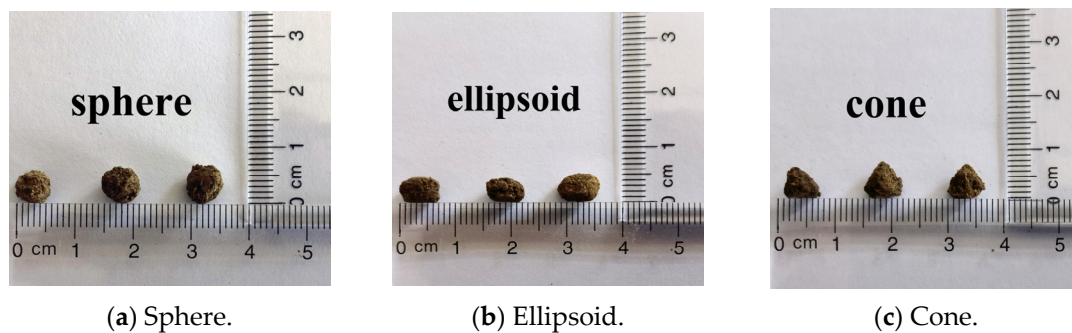


Figure 3. Three different shapes of soil particles.

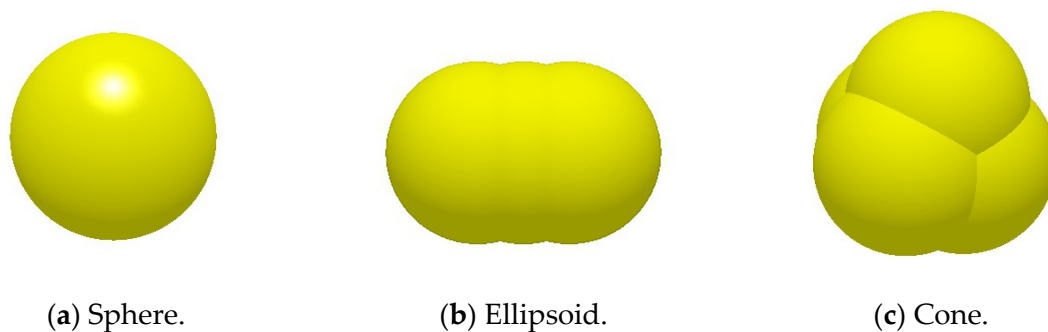


Figure 4. Simulation model of three different shapes of soil particles.

2.5. Soil AoR Test

Due to the strong cohesiveness of soda saline–alkali soil in the Songnen Plain of Northeast China, we used the cylinder pulling method to measure the static angle of repose by a 65 Mn steel cylinder with a diameter of 80 mm and a height of 250 mm. During the test, the cylinder was pulled at a constant speed of 0.1 m/s. After conducting the test for 5 repetitions, the static angle of repose of the soil was determined to be 44.32° , with a standard deviation of 2.001° , as shown in Figure 5.

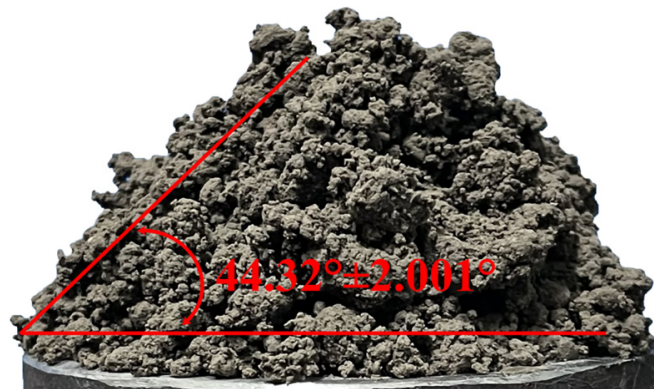


Figure 5. Soil AoR test.

2.6. Calibration of the DEM Parameters of the Soda Saline–Alkali Soil

Numerous parameters exert influence on the static angle of repose of soil. In this study, we initially conducted the Plackett–Burman (PB) test to identify the most significant parameters impacting the static angle of repose of soil. Subsequently, the steepest ascent (SA) test was employed to narrow down the range of these influential parameters. Following this, a quadratic regression orthogonal test was executed to formulate a multiple regression equation. The optimal combination of simulation parameters, tailored to the soda saline–alkali soil of the Songnen Plain, was determined through the solution optimization of this equation. Finally, the obtained parameter combinations were used to simulate the soil rest angle accumulation test and compared with the experimental values. Table 1 shows the high (+1) and low (−1) levels of parameters *A–I* in the PB test.

Table 1. High and low levels of the PB test.

Simulation Test Parameters	Low Level	High Level
<i>A</i> (Poisson's ratio)	0.3	0.5
<i>B</i> (shear modulus)	1×10^6	5×10^6
<i>C</i> (soil–soil restitution coefficient)	0.1	0.3
<i>D</i> (soil–soil static friction coefficient)	0.3	0.9
<i>E</i> (soil–soil rolling friction coefficient)	0.1	0.3
<i>F</i> (soil–65Mn steel restitution coefficient)	0.1	0.3
<i>G</i> (soil–65Mn steel static friction coefficient)	0.3	0.9
<i>H</i> (soil–65Mn steel rolling friction coefficient)	0.1	0.3
<i>I</i> (JKR surface energy)	0.1	1

Based on EDEM software (EDEM version: EDEM 2018, DEM Solutions, Edinburgh, UK, 2002), a soil particle model was established using a multisphere combination method for simulation experiments [32–34], which cannot reflect the magnitude of the soil water content. The bonding between particles needed to be characterized by the JKR surface energy, which was subsequently calibrated by the simulation test in this paper, and the Rayleigh time step of the simulation test was 1.5×10^{-4} s. The simulation screenshot of the soil AoR test is shown in Figure 6 below.

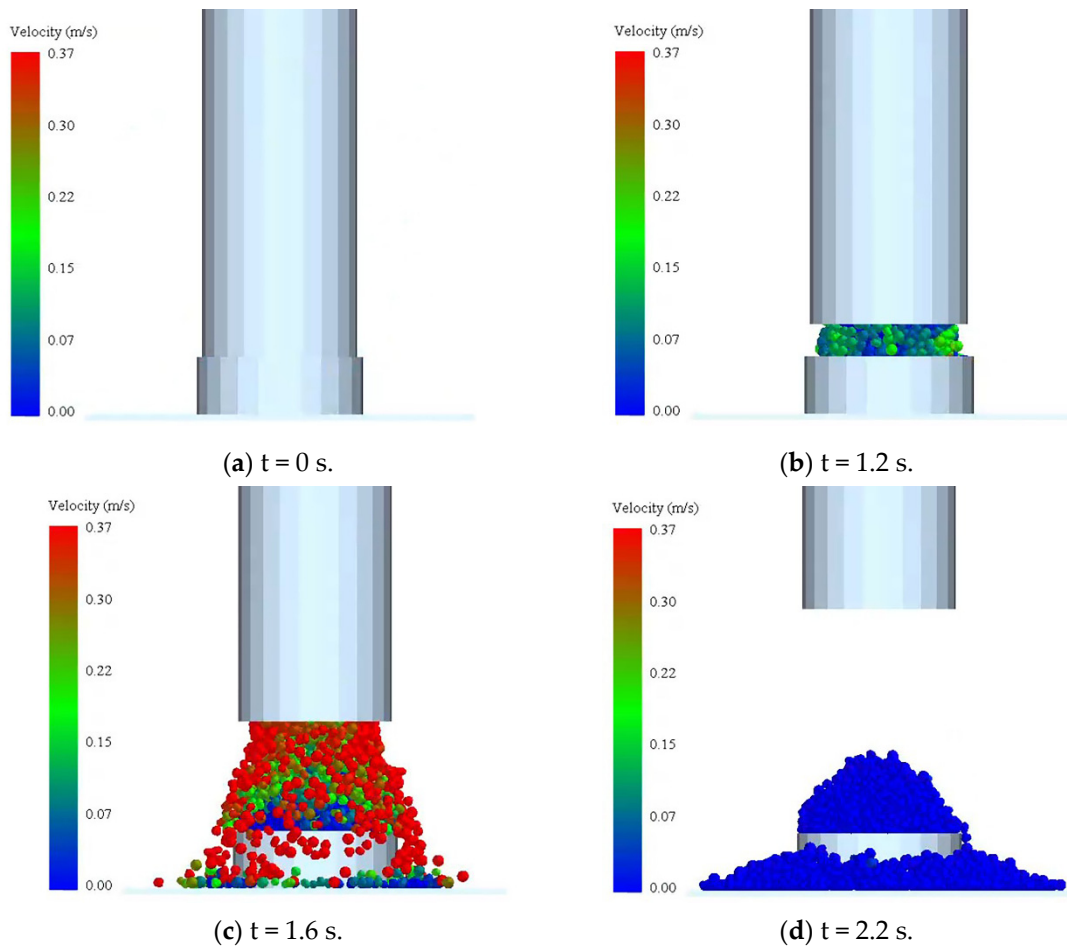
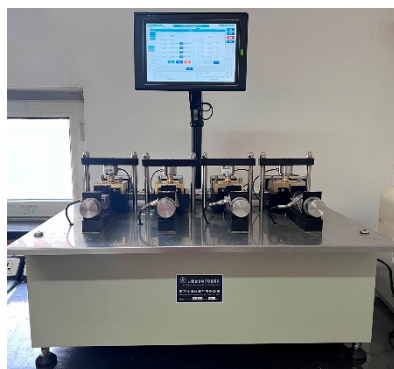


Figure 6. Simulation screenshot of the soil AoR test.

2.7. DS Test

The accuracy and effectiveness of the simulation parameters were further verified by the direct shear test. As shown in Figure 7, a ZJ-type automatic quadruple direct shear tester was used to determine the shear strength of soil under four vertical loads (50, 100, 200, and 300 kPa) in soda saline soils in the northeast. Three soil specimens were taken for each vertical pressure, and three tests were conducted. The test data were recorded to obtain the soil shear strength versus vertical load curves under different vertical pressures.



(a) ZJ-type automatic quadruple direct shear tester.



(b) Soil samples after direct shear.

Figure 7. DS physical test.

3. Results and Discussion

3.1. Soda Saline–Alkali Soil Particle Size and pH Value

The test results are shown in Figures 8 and 9. In Figure 8, the particle size distribution under the tillage layer is roughly the same, except for the surface layer of soda saline–alkali soil at 0–10 cm, where the particle size distribution is special. The soda saline–alkali soil sample texture is sandy loam. Figure 9 shows the soda saline–alkali soil pH value test results under different tillage layers. It can be seen in the Figure 9 that the soil particles are alkaline under the 0–10 cm tillage layer.

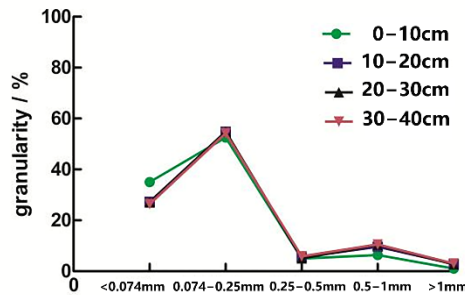


Figure 8. Particle size of soda saline–alkali soil under different tillage layers.

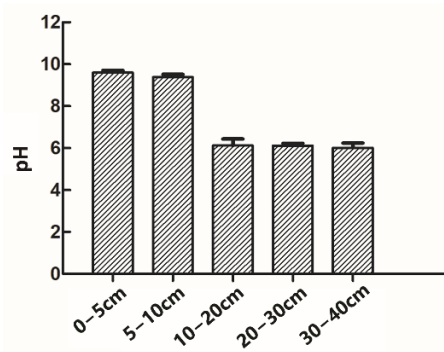


Figure 9. pH value of soda saline–alkali soil under different tillage layers.

3.2. Water Content, Density, and Firmness Test Results of Soda Saline–Alkali Soil

Figure 10 shows the soda saline–alkali soil moisture content under different tillage layers. It can be seen in the figure that the moisture content increases slowly with the deepening of the tillage layer.

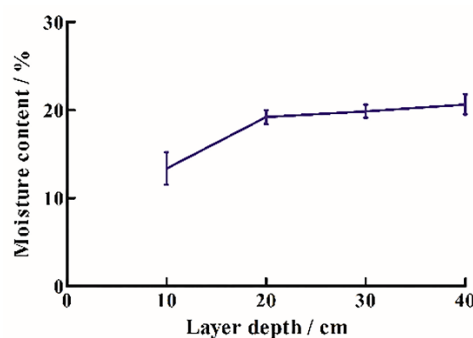


Figure 10. Moisture content of soda saline–alkali soil under different plow layers.

Figure 11 shows the density of soda saline–alkali soil under different plow layers. It can be seen in the figure that the density increases with the deepening of the plow layer.

The results of the SA test are shown in Table 3. At the level of the No. 3 test, when D was 0.6, E was 0.2, and I was 0.55, the static angle of repose was $44.44^\circ \pm 0.82$, the static angle of repose of the physical test was $44.32^\circ \pm 2.001$, and the minimum relative error was 0.28%. The No. 3 test level was used as the central point in the subsequent experiments, and No. 2 and No. 3 were used as low and high levels for the experimental design.

Table 3. Design and results of the SA test.

No.	D	E	I	Repose Angle $\theta/(^\circ)$	Relative Error (%)
1	0.9	0.1	0.1	35.58 ± 1.63	19.72
2	0.75	0.15	0.325	37.23 ± 1.93	16
3	0.6	0.2	0.55	44.44 ± 0.82	0.28
4	0.45	0.25	0.725	48.18 ± 1.69	8.71
5	0.3	0.3	1	49.18 ± 1.70	10.97

Finally, we conducted the BB test. The test parameter level is shown in Table 4, the test design and results are shown in Table 5, and the nonsignificant parameters are the same as the SA test.

Table 4. Table of parameter levels of the BB test.

Levels	Soil–Soil Static Friction Coefficient D	Soil–Soil Rolling Friction Coefficient E	JKR Surface Energy I
−1	0.45	0.15	0.325
0	0.6	0.2	0.525
+1	0.75	0.25	0.725

Table 5. Design and results of the BB test.

No.	Soil–Soil Static Friction Coefficient D	Soil–Soil Rolling Friction Coefficient E	JKR Surface Energy I	Repose Angle $\theta/(^\circ)$
1	−1	−1	0	44.33
2	1	−1	0	46.59
3	−1	1	0	43.71
4	1	1	0	42.43
5	−1	0	−1	44.97
6	1	0	−1	42.8
7	−1	0	1	42.83
8	1	0	1	47.23
9	0	−1	−1	44.63
10	0	1	−1	41.12
11	0	−1	1	43.68
12	0	1	1	44.27
13	0	0	0	43.17
14	0	0	0	42.77
15	0	0	0	42.43
16	0	0	0	42.36
17	0	0	0	42.02

From the BB test ANOVA (shown in Appendix A, Table A2), we can see that D (soil–soil static friction coefficient), E (soil–soil rolling friction coefficient), and I (soil surface energy) have significant effects on the static angle of repose. The parameters D (soil–soil static friction coefficient) and I (soil surface energy) have more significant effects on the static angle of repose than E (soil–soil rolling friction coefficient).

Additionally, from the relationship curve between the experimental values and the predicted values of the fitted model (Figure 13), it can be seen that the data points are distributed around the fitted line with small errors, indicating that the model fits well and can be used for a predictive analysis of the static rest angle.

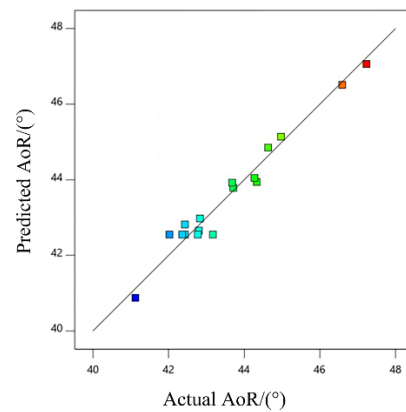


Figure 13. Relationship curve between the actual value and predicted value of soil AoR.

The response surface analysis of the regression model can obtain the influence of the interaction of various factors on the angle of repose, where the regression model of the angle of repose and each significant parameter can be described as Equation (8). Taking the physical repose angle ($44.32^\circ \pm 2.001$) of soda saline–alkali soil in Northeast China as the target value and then solving the regression model, the parameter range can be determined as follows:

$$AoR = 42.55 - 0.9625D + 0.4013E + 0.5613I - 0.8850DE + 1.03DJ + 1.64EJ + 0.3412D^2 + 1.37E^2 + 0.5337I^2 \quad (8)$$

$$AoR = 44.32^\circ \quad (9)$$

$$\begin{cases} 0.45 \leq D \leq 0.75 \\ 0.15 \leq E \leq 0.25 \\ 0.325 \leq I \leq 0.725 \end{cases} \quad (10)$$

Using Design-Expert 11.0 software and taking the angle of repose of the physical experiment as the target value, the second-order regression equation was obtained by analyzing the BB experimental data. The equation was optimized to obtain a set of parameters: the soil–soil static friction coefficient was 0.734, the soil–soil rolling friction coefficient was 0.151, the *JKR* surface energy was 0.56, and the other nonsignificant parameters were the same as the steepest climbing test.

The best parameter combination was used as the EDEM simulation parameter to verify the accuracy and reliability of soil parameter calibration. The static AoR simulation test was conducted many times. The average static AoR of the soil is 44.034° , the standard deviation is 0.911° , the physical static AoR is 44.32° , the standard deviation is 2.001° , and the relative error is 0.645%, as shown in Figure 14; there is no significant difference between the simulated and the physical static AoR of the soil.

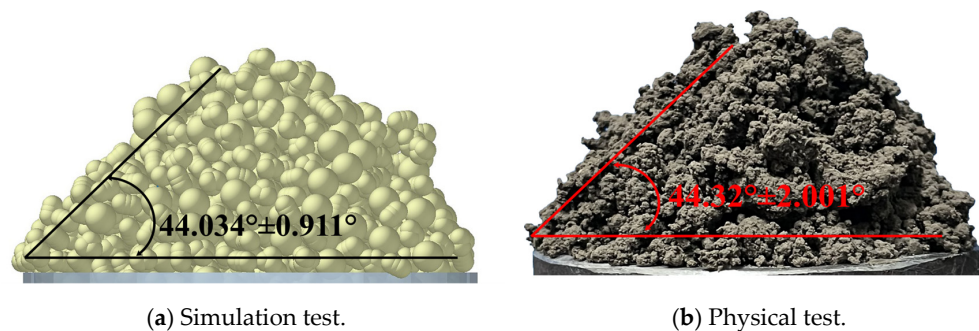


Figure 14. Comparison of simulation static AoR test and physical static AoR test results.

3.4. DS Test Simulation Results

The DS simulation test is shown in Figure 15, using the combination of parameters obtained from the calibration. The plate was added to apply pressure to the soil sample to simulate different vertical loads in the DS test, and the total shear duration was set to 7 s. When the simulation is 1.5 s, the soil particles have been completely generated. At 1.5 s in the simulation, the plate begins to load in the +Z direction. At 2.5 s, the down box begins to move along the +X direction at a speed of 0.002 m/s until the end of the simulation. The soil shear strength was obtained by exporting the data through the postprocessing module of EDEM software (EDEM version: EDEM 2018, DEM Solutions, Edinburgh, UK, 2002) [35].

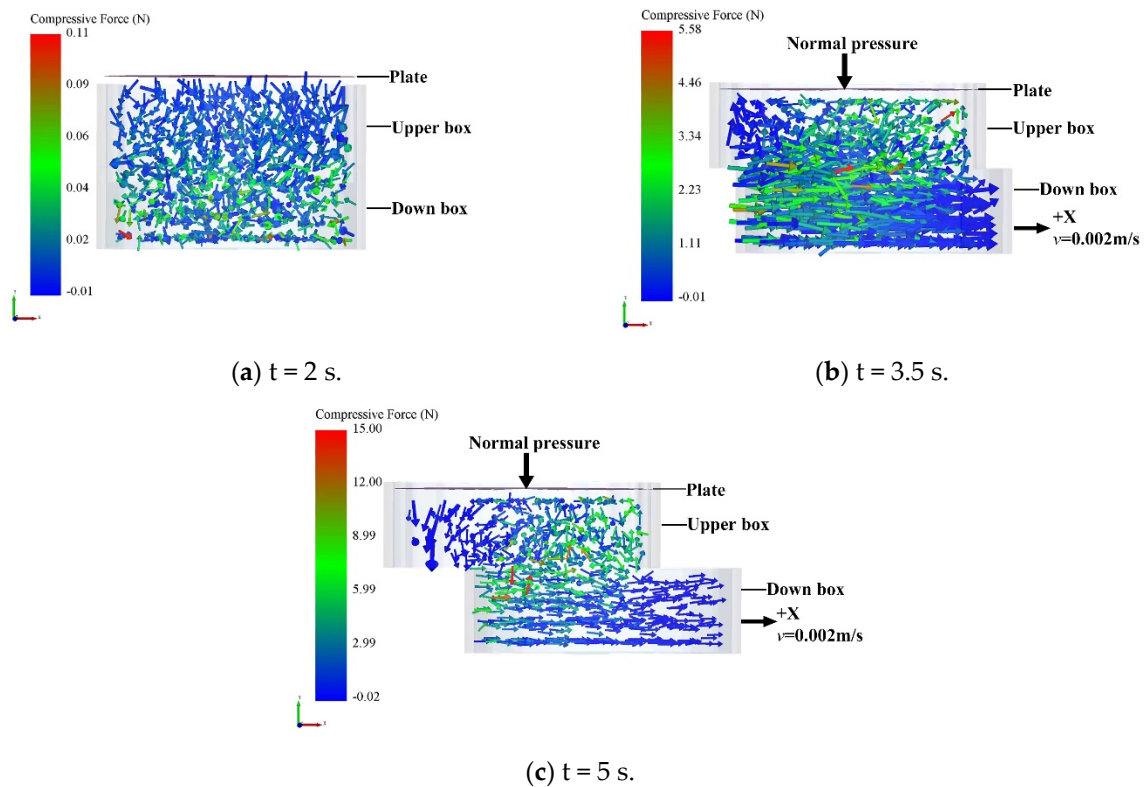


Figure 15. Screenshot of the DS test simulation.

The vertical load–shear strength comparison curve of the physical test and simulation test is shown in Figure 16. In the figure, it can be seen that the two trends are the same, but the shear strength obtained from the simulation deviates from the physical test results. The simulation parameters need to be further corrected.

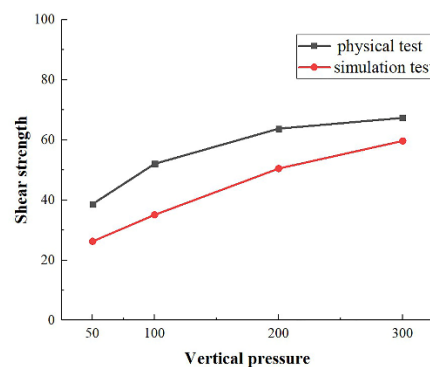


Figure 16. Comparison of simulation results and physical results.

3.5. Contact Model and Parameter Correction

To enhance the validation’s reliability, we employed two distinct validation methods: the angle of repose (AoR) test and the direct shear (DS) test. During the verification process, it became evident that employing the same set of simulation parameters yielded different outcomes for these two tests. After that, we modified the relevant model parameters. Equation (11) is the calculation formula of model-related parameters.

$$\begin{cases} \Delta F_n = -v_n S_n A_b \Delta t \\ \Delta F_\tau = -v_\tau S_\tau A_b \Delta t \\ \Delta M_n = -\omega_n S_n J \Delta t \\ \Delta M_\tau = -\omega_\tau S_\tau \frac{J}{2} \Delta t \\ A_b = \pi R_b^2 \\ J = \frac{1}{2} \pi R_b^4 \end{cases} \quad (11)$$

In Equation (11), A_b is the contact area between soil particles, m^2 ; R_b is the bond radius between soil particles, m ; J is the cross-sectional polar moment of inertia of soil particles, m^4 ; S_n is the normal stiffness of bonded particles, N/m^3 ; S_τ is the tangential stiffness of bonded particles, N/m^3 ; v_n and v_τ are the normal and tangential components of particle velocity, m/s ; ω_n and ω_τ are the normal and tangential components of particle angular velocity, rad/s ; and Δt is the time step, s .

When the external force exceeds a preset value, the bond is destroyed. The normal critical stress, σ_{max} , and the tangential critical stress, τ_{max} , are defined as follows:

$$\sigma_{max} = \frac{-F_n}{A} + \frac{2M_\tau}{J} R_b \quad (12)$$

$$\tau_{max} = \frac{-F_\tau}{A} + \frac{M_n}{J} R_b \quad (13)$$

The bond parameters in the HMB contact model mainly include the normal stiffness, S_n ; tangential stiffness, S_τ ; critical normal stress, σ_{max} ; critical tangential stress, τ_{max} ; and bond radius, R_b . Previous studies have shown that the particle behavior is not sensitive to the change of bond stiffness parameters under this model [6]. After multiple pre-tests, the normal stiffness per unit area is taken as $1 \times 10^5 \text{ N/m}^3$, the tangential stiffness per unit area is taken as $1 \times 10^5 \text{ N/m}^3$, and $\sigma_{max} = \tau_{max}$ is $8 \times 10^3 \text{ Pa}$. The particle contact radius is 1.1 times the particle radius [12].

Meanwhile, the shear modulus affects the time step variation of the DEM solution [36]; the larger the shear modulus is, the smaller the Rayleigh time step, according to Equation (13). In general, the smaller the time step is, the more time the calculation will take, and the higher the calculation accuracy will be [37]. To obtain an accurate combination of simulation parameters, we adjusted the shear modulus and Rayleigh time step to obtain more accurate calculation results for subsequent simulations. In the direct shear simulation test, the Rayleigh time step is $4.76 \times 10^{-5} \text{ s}$, and the shear modulus is $3 \times 10^7 \text{ Pa}$.

$$T_r = \frac{\pi R \sqrt{\frac{\rho}{G}}}{0.1631v + 0.8766} \quad (14)$$

In Equation (14), T_r is the Rayleigh time step, R is the particle radius, ρ is the particle density, v is Poisson’s ratio, and G is the shear modulus.

After modifying the model parameters and conducting the DS simulation again (Figure 17), it is obvious that the bonds between soil particles were constantly broken during the DS test process. Because the bonds between soil particles have a certain strength, the simulated shear strength is improved compared with the single JKR model. The simulation results with a small relative error with the physical test were obtained, as shown in Figure 18.

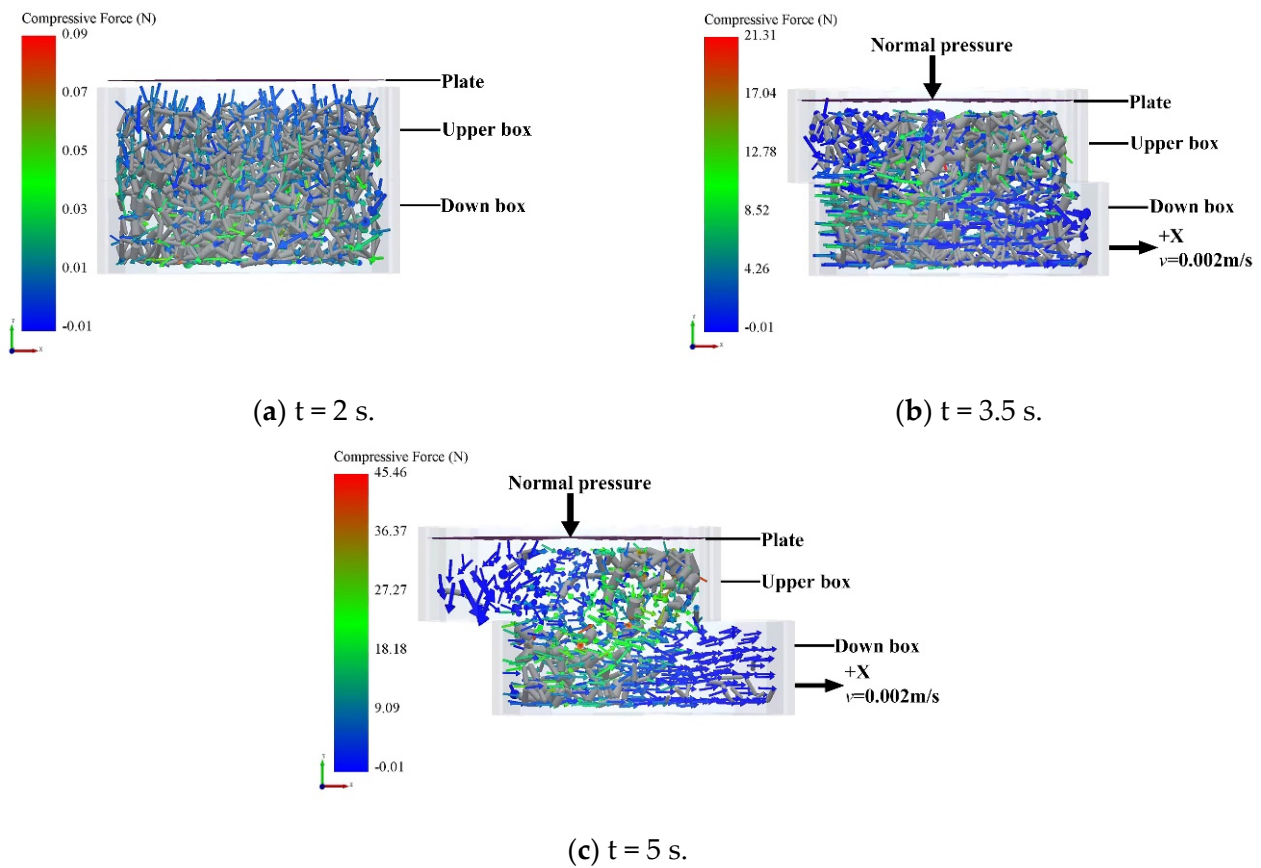


Figure 17. Simulation screenshot of DS test after correction.

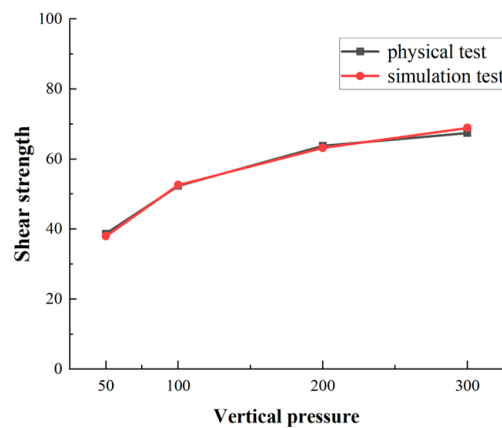


Figure 18. Comparison of simulation results and physical results after correction.

This simulation parameter combination is used to simulate the AoR test again, as shown in Figure 19. After multiple tests, the static angle of repose is 44.2° , and the standard deviation is 1.406° , which is not significantly different from the physical test angle of repose of 44.32° and the standard deviation of 2.001° , which verifies the reliability of the obtained parameter combination. Table 6 shows the calibrated soil simulation parameters.

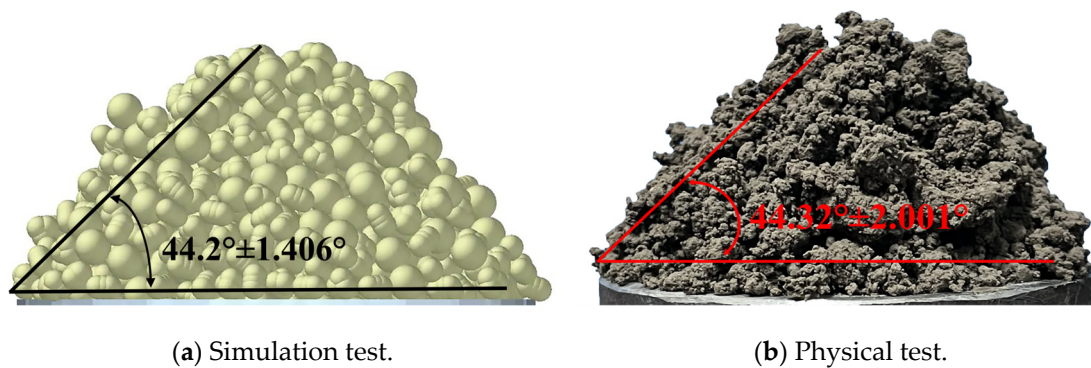


Figure 19. Comparison of static AoR between simulation test and physical test after correction.

Table 6. Soil simulation parameters table.

Simulation Test Parameters	Value
Density	2650 kg/m ³
Poisson's ratio	0.4
shear modulus	3×10^7 Pa
Soil–soil restitution coefficient	0.2
Soil–soil static friction coefficient	0.734
Soil–soil rolling friction coefficient	0.151
Soil–65Mn steel restitution coefficient	0.2
Soil–65Mn steel static friction coefficient	0.6
Soil–65Mn steel rolling friction coefficient	0.2
JKR surface energy	0.33 J/m ²
Normal stiffness per unit area	1×10^5 N/m ³
Shear stiffness per unit area	1×10^5 N/m ³
Critical normal stress	8×10^3 Pa
Critical shear stress	8×10^3 Pa
Bonded disk radius	5 mm

3.6. Discussion

In this study, the contact parameters between soda saline–alkali and soil–subsoiling components in Northeast China were calibrated. Based on the DEM, the JKR model and HMB model were used as contact models, and the accuracy of the calibrated contact parameter combination was verified by the AoR test and DS test.

Through the PB test results (Table A1), it can be found that both the soil intrinsic parameters and the contact parameters will affect the AoR. The contact parameters between the soils (soil–soil rolling friction coefficient, soil–soil static friction coefficient, and JKR surface energy of the soil) have a more significant effect on the AoR, and the JKR surface energy of the soil has a greater effect than the static friction coefficient and the rolling friction coefficient; the results are similar to those of Xing et al. [19]. After that, the SA test and BB test were conducted on the parameters with significant influence, and the BB tests were analyzed by ANOVO (Table A2). The results showed a model p -value < 0.001; a coefficient of determination of $R^2 = 0.9661$; a coefficient of determination adjusted of $R^2 = 0.9225$, close to 1; and a coefficient of variation of C.V. = 1.02%, thus indicating a significant relationship between the response values and the parameters. Through the ANOVO analysis, it can be seen that the interaction of two significant parameters will also have a significant impact on the angle of repose. The interaction term containing soil JKR surface energy is more significant than other interaction terms. The results of this study are similar to those of Hao, Li, et al. [16,18]. We speculate that because the soil moisture content cannot be characterized when the EDEM software (EDEM version: EDEM 2018, DEM Solutions, Edinburgh, UK, 2002) is used to simulate the soil particles, when the JKR model is used as the simulation contact model, the soil moisture content can only be simulated by

changing the surface energy of the JKR, which also indicates that the soil water content has a large effect on its AoR and friction coefficient.

When using EDEM to calibrate soil contact parameters, most scholars use the angle of repose as the response value and use a single contact model as the contact model [6,14,17,21,23]. However, during the subsoiling process, the soil is sheared by the subsoiling components. Taking this into account, we conducted direct shear tests to verify the calibrated contact parameters. The results show that there is a certain error between the simulation results of the direct shear test and the physical test results when only using the JKR model as the contact parameter obtained by the contact model (Figure 16). This discrepancy can be attributed to the fact that the AoR test and DS test characterize the soil's flow and shear characteristics, respectively. A single model cannot precisely simulate both aspects of soil behavior. Through repeated experiments, it was found that the addition of bonds between soil particles to simulate the characteristics of high hardness and easy hardening of saline–alkali soil in Northeast China can obtain results closer to physical experiments. Notably, these bonds between soil particles can be disrupted during the DS test. However, even in the event of bond disruption during the shear process, the soil retains cohesion due to the surface energy. In order to faithfully reflect the shear and flow characteristics of the soil particle population, we conducted the DS test by amalgamating the JKR contact model and the HMB contact model, thereby modifying the discrete element simulation parameters.

We used the modified parameter combination to carry out the repose angle simulation test and the direct shear simulation test, and the results are very close to those of the physical test. Therefore, future research could consider combining multiple contact models to simulate different mechanical properties of soil to obtain more accurate simulation results.

4. Conclusions

This study utilized DEM to model saline soil particles with a multisphere combination approach and validated the model's accuracy using soda saline soil from Northeast China's Songnen Plain. We introduced a modeling method for individual soil particles based on their geometric shape. The effectiveness of this method was confirmed through comparisons between simulation results and experimental data from the angle of repose (AoR) and direct shear tests.

1. The physical properties of the soil, including the texture, density, water content, and particle size distribution, were tested. According to the test analysis, the soil studied in this paper is sandy loam.
2. Most soil particles can be approximated as spheres, ellipsoids, and cones. Based on the above three shapes, the geometric model of soil particles was established using the method of multisphere combination. Considering the adhesion between soil particles, the JKR model was used to calculate the force between particles.
3. The simulation parameters were calibrated by the soil AoR test. The results of the PB test showed that the static friction coefficient, rolling friction coefficient, and JKR surface energy between saline–alkali soil particles in Northeast China significantly affected the static angle of repose. Then, SA and BB tests were carried out to further determine the optimal parameter combination for soda saline–alkali soil simulation in Northeast China. ANOVA was used to analyze the BB test results, a quadratic regression model was established, and the model fit was good. The results showed that the soil–soil static friction coefficient, rolling friction coefficient, and JKR surface energy and parameters significantly affected the resting angle by a two–two interaction.
4. Sensitivity parameters were refined using a combination of the JKR and HMB contact models. The modified contact parameters are as follows: JKR surface energy is 0.33 J/m^2 , soil–soil static friction coefficient is 0.734, and soil–soil rolling friction coefficient is 0.151. The bonding parameters are as follows: normal stiffness per unit area is $1 \times 10^5 \text{ N/m}^3$, shear stiffness per unit area is $1 \times 10^5 \text{ N/m}^3$, critical normal stress is $8 \times 10^3 \text{ Pa}$, and critical shear stress is $8 \times 10^3 \text{ Pa}$. Using the modified

parameter combinations for simulation and comparison with the physical tests, the simulation results closely matched the trend and values of the shear strength curve obtained in physical testing. The static repose angle obtained by simulation is 44.2° , and the standard deviation is 1.405° ; it is not significantly different from the static AoR of the physical test, which is 44.32° , and the standard deviation is 2.001° . Thus, the reliability and accuracy of the obtained parameter combination were verified.

Author Contributions: The seven authors developed the research approach together. M.L., conceptualization and writing—original draft; J.W., writing—review and editing; W.F., formal analysis; writing—review and editing; H.J., formal analysis; writing—review and editing; Y.W., formal analysis; writing—review and editing; Y.G., formal analysis; writing—review and editing; T.X., formal analysis; writing—review and editing. All authors have read and agreed to the published version of the manuscript.

Funding: This research was funded by [Science and Technology Research Project of Jilin Provincial Department of Education], grant number [JJKH20210339KJ], and [Development of supporting equipment for ecological improvement of soda saline-alkali land in Northeast China], grant number [20210202018NC].

Data Availability Statement: All data analyzed during this study are included in this article.

Acknowledgments: In this paper, we received technical support from the College of biological and agricultural engineering in Jilin University, including the Licensed software of EDEM and the coupling interface.

Conflicts of Interest: The authors declare no conflict of interest.

Nomenclature

AoR	Angle of repose
A_b	Contact area between soil particles, m^2
BB	Box–Behnken test
DEM	Discrete element method
E^*	Equivalent elastic modulus, Pa
E_1	Elastic modulus of particle 1, Pa
E_2	Elastic modulus of particle 2, Pa
F_{JKR}	JKR normal contact force, N
F_t^c	Tangential contact force, N
F_n^d	Normal damping force, N
F_t^d	Tangential damping force, N
G	Shear modulus
HM	Hertz–Mindlin (no slip) model
J	Cross-sectional polar moment of inertia of soil particles, m^4
JKR	Hertz–Mindlin (with Johnson–Kendall–Roberts) model
PB	Plackett–Burman test
R^*	Equivalent contact radius, m
R_1	Contact radius of particle 1, m
R_2	Contact radius of particle 2, m
R	Particle radius
R_b	Bond radius between soil particles, m
SA	Steepest ascent test
S_n	Normal stiffness of bonded particles, N/m^3
S_τ	Tangential stiffness of bonded particles, N/m^3
Tr	Rayleigh time step
δ_n	Normal overlap, m
δ_t	Tangential overlap, m
α	Contact radius, m
γ	Surface energy, N/m
ν	Poisson's ratio

v_n	Normal component of relative velocity of particles, m/s
v_t	Tangential component of relative velocity of particles, m/s
v_1	Poisson's ratio of particle 1
v_2	Poisson's ratio of particle 2
v_n	Normal components of particle velocity, m/s
v_τ	Tangential components of particle velocity, m/s
ρ	Particle density
ω_n	Normal components of particle angular velocity, rad/s
ω_τ	Tangential components of particle angular velocity, rad/s
Δt	Time step, s

Appendix A

Table A1. ANOVA of PB test.

Parameters	Degree of Freedom	Sum of Squares	F-Value	<i>p</i> -Value
Model	9	354.35	53.07	0.0186
A	1	29.11	39.24	0.0246
B	1	15.99	21.55	0.0434
C	1	9.77	13.17	0.0682
D	1	40.96	55.21	0.0176
E	1	36.16	48.74	0.0199
F	1	17.89	24.11	0.0391
G	1	0.1704	0.2297	0.6790
H	1	0.0374	0.0504	0.8432
I	1	204.27	275.33	0.0036

Table A2. ANOVA of BB test.

Source	Mean Square	Degree of Freedom	Sum of Square	<i>p</i> -Value
Model	4.41	9	39.69	0.0002
D	7.41	1	7.41	0.0005
E	1.29	1	1.29	0.0384
I	2.52	1	2.52	0.0092
DE	3.13	1	3.13	0.0054
DI	4.20	1	4.20	0.0025
EI	10.79	1	10.79	0.0002
D ²	0.4903	1	0.4903	0.1605
E ²	7.95	1	7.95	0.0004
I ²	1.20	1	1.20	0.0438
Residual	0.1990	7	1.39	
Lack of fit	0.2096	3	0.6288	0.4472
Pure error	0.1910	4	0.7642	
Sum		16	41.08	

References

- Coetzee, C.J. Review: Calibration of the discrete element method. *Powder Technol.* **2017**, *310*, 104–142. [[CrossRef](#)]
- Cundall, P.A.; Strack, O.A. Discrete numerical model for granular assemblies. *Géotechnique* **2008**, *30*, 331–336. [[CrossRef](#)]
- Zeng, Z.; Ma, X.; Cao, X.; Li, Z.; Wang, X. Critical Review of Applications of Discrete Element Method in Agricultural Engineering. *Trans. Chin. Soc. Agric. Mach.* **2021**, *52*, 1–20.
- He, Y.; Wu, M.; Xiang, W.; Yan, B.; Wang, J.; Bao, P. Application Progress of Discrete Element Method in Agricultural Engineering. *Chin. Agric. Sci. Bull.* **2017**, *33*, 133–137.
- Zhong, W.; Yu, A.; Liu, X.; Tong, Z.; Zhang, H. DEM/CFD-DEM Modelling of Non-spherical Particulate Systems: Theoretical Developments and Applications. *Powder Technol.* **2016**, *302*, 108–152. [[CrossRef](#)]
- Wang, X.; Hu, H.; Wang, Q.; Li, H.; He, J.; Chen, W. Calibration Method of Soil Contact Characteristic Parameters Based on DEM Theory. *Trans. Chin. Soc. Agric. Mach.* **2017**, *48*, 78–85.
- Ma, Z.; Cao, Y.; Wang, Q. Effects of Planting Rice on Soil Physical and Chemical Properties of Saline-alkali Land in Northern Shaanxi and Screening of Saline-alkali-tolerant Rice Varieties. *China Rice* **2022**, *28*, 80–83+87.

8. Wang, Q.; Lu, N.; Wei, Y. Effects of different improvement measures on soil physicochemical properties and growth and yield of ryegrass in saline-alkali soils of Dingbian area. *Jiangsu Agric. Sci.* **2019**, *47*, 282–286.
9. Wang, Z.; Wang, H.; Ma, X.; Wang, Q.; Wang, Z. Effects of adding bio-organic fertilizer on maize yield and soil physical and chemical properties in saline-alkali soil. *Mod. Agric.* **2022**, *9*, 21–23.
10. Zhang, X.; Liu, S.; Sun, Y.; Hu, A.; Li, K.; Chen, Y. Variation Characteristics of Soil Physicochemical Properties of Coastal Saline-alkali Lands with Different Improvement Years. *Res. Soil Water Conserv.* **2022**, *29*, 113–118.
11. Zhang, X. *Effects of Different Straw Return Patterns on the Physicochemical Properties and Carbon Pool of Saline Soils*; Harbin Normal University: Harbin, China, 2022.
12. Carmine, P.; Angelo, C. Squeeze lubrication between soft solids: A numerical study. *Tribol. Int.* **2022**, *176*, 107824.
13. Jaeger, H.M.; Nagel, S.R.; Behringer, R.P. The physics of granular materials. *Phys. Today* **1996**, *49*, 32–38. [[CrossRef](#)]
14. Yang, Q.Z.; Shi, L.; Shi, A.P.; He, M.S.; Zhao, X.Q.; Zhang, L.; Addy, M. Determination of key soil characteristic parameters using angle of repose and direct shear stress test. *Int. J. Agric. Biol. Eng.* **2023**, *16*, 143–150. [[CrossRef](#)]
15. Asaf, Z.; Rubinstein, D.; Shmulevich, I. Determination of discrete element model parameters required for soil tillage. *Soil Tillage Res.* **2007**, *92*, 227–242. [[CrossRef](#)]
16. Hao, B.; Tong, X.; Chen, Z.; Liu, H. Calibration of simulation parameters for wind erosion gas-solid two-phase flow in arid and semiarid soils. *Rev. Bras. De Eng. Agrícola E Ambient.* **2022**, *26*, 564–570. [[CrossRef](#)]
17. Zhu, J.; Zou, M.; Liu, Y.; Gao, K.; Su, B.; Qi, Y. Measurement and calibration of DEM parameters of lunar soil simulant. *Acta Astronaut.* **2022**, *191*, 169–177. [[CrossRef](#)]
18. Li, J.; Tong, J.; Hu, B.; Wang, H.; Mao, C.; Ma, Y. Calibration of parameters of interaction between clayey black soil with different moisture content and soil-engaging component in northeast China. *Trans. Chin. Soc. Agric. Eng.* **2019**, *35*, 130–140.
19. Xing, J.; Zhang, R.; Wu, P.; Zhang, X.; Dong, X.; Chen, Y.; Ru, S. Parameter calibration of discrete element simulation model for latosol particles in hot areas of Hainan Province. *Trans. Chin. Soc. Agric. Eng.* **2020**, *36*, 158–166.
20. Du, J.; Heng, Y.; Zheng, K.; Luo, C.; Zhu, Y.; Zhang, J.; Xia, J. Investigation of the burial and mixing performance of a rotary tiller using discrete element method. *Soil Tillage Res.* **2022**, *220*, 105349. [[CrossRef](#)]
21. Hang, C.G.; Gao, X.J.; Yuan, M.C.; Huang, Y.X.; Zhu, R.X. Discrete element simulations and experiments of soil disturbance as affected by the tine spacing of subsoiler. *Biosyst. Eng.* **2017**, *168*, 73–82. [[CrossRef](#)]
22. Ono, I.; Nakashima, H.; Shimizu, H.; Miyasaka, J.; Ohdoi, K. Investigation of elemental shape for 3D DEM modeling of interaction between soil and a narrow cutting tool. *J. Terramechanics* **2013**, *50*, 265–276. [[CrossRef](#)]
23. Li, B.; Chen, Y.; Chen, J. Modeling of soil-claw interaction using the discrete element method (DEM). *Soil Tillage Res.* **2016**, *158*, 177–185. [[CrossRef](#)]
24. Shmulevich, I. State of the art modeling of soil-tillage interaction using discrete element method. *Soil Tillage Res.* **2010**, *111*, 41–53. [[CrossRef](#)]
25. Shmulevich, I.; Rubinstein, D.; Asaf, Z. Discrete Element Modeling of Soil-Machine Interactions. *Adv. Soil Dyn.* **2009**, *3*, 399–433.
26. Wang, X.Z.; Zhang, S.; Pan, H.B.; Zheng, Z.Q.; Huang, Y.X.; Zhu, R.X. Effect of soil particle size on soil-subsoiler interactions using the discrete element method simulations. *Biosyst. Eng.* **2019**, *182*, 138–150. [[CrossRef](#)]
27. Song, Z.; Li, H.; Yan, Y.; Tian, F.; Li, Y.; Li, F. Calibration Method of Contact Characteristic Parameters of Soil in Mulberry Field Based on Unequal-diameter Particles DEM Theory. *Trans. Chin. Soc. Agric. Mach.* **2022**, *53*, 21–33.
28. Zhang, J.; Xia, M.; Chen, W.; Yuan, D.; Wu, C.Y.; Zhu, J.P. Simulation Analysis and Experiments for Blade-Soil-Straw Interaction under Deep Ploughing Based on the Discrete Element Method. *Agriculture* **2023**, *13*, 136. [[CrossRef](#)]
29. Zhang, H. *Experimental Study on Vibration Subsoiling Components in Soda Saline-alkali Soil*; Jilin Agricultural University: Changchun, China, 2022.
30. Johnson, K.L.; Kendall, K.; Roberts, A.D. Surface energy and the contact of elastic solids. *Proc. R. Soc. Lond. A Math. Phys. Sci.* **1971**, *324*, 301–313.
31. Santos, K.G.; Campos, A.; Oliveira, O.S.; Ferreira, L.; Francisquetti, M. DEM simulations of dynamic angle of repose of acerola residue: A parametric study using a response surface technique. *Blucher Chem. Eng. Proc.* **2015**, *1*, 11326–11333.
32. Xu, T.; Zhang, R.; Wang, Y.; Jiang, X.; Feng, W.; Wang, J. Simulation and Analysis of the Working Process of Soil Covering and Compacting of Precision Seeding Units Based on the Coupling Model of DEM with MBD. *Processes* **2022**, *10*, 1103. [[CrossRef](#)]
33. Xu, T.; Zhang, R.; Jiang, X.; Feng, W.; Wang, Y.; Wang, J. Study on Verification Approach and Multicontact Points Issue When Modeling *Cyperus esculentus* Seeds Based on DEM. *Processes* **2023**, *11*, 825. [[CrossRef](#)]
34. Xu, T.; Zhang, R.; Zhu, F.; Feng, W.; Wang, Y.; Wang, J. A DEM-Based Modeling Method and Simulation Parameter Selection for *Cyperus esculentus* Seeds. *Processes* **2022**, *10*, 1729. [[CrossRef](#)]
35. Ucgul, M.; Fielke, J.M.; Saunders, C.J.B.E. Three-dimensional discrete element modelling (DEM) of tillage: Accounting for soil cohesion and adhesion. *Biosyst. Eng.* **2015**, *129*, 298–306. [[CrossRef](#)]

36. Cunha, R.N.; Santos, K.G.; Lima, R.N.; Duarte, C.R.; Barrozo, M.A.S. Repose angle of monoparticles and binary mixture: An experimental and simulation study. *Powder Technol.* **2016**, *303*, 203–211. [[CrossRef](#)]
37. Burns, S.J.; Hanley, K.J. Establishing stable time-steps for DEM simulations of non-collinear planar collisions with linear contact laws. *Int. J. Numer. Methods Eng.* **2017**, *110*, 186–200. [[CrossRef](#)]

Disclaimer/Publisher’s Note: The statements, opinions and data contained in all publications are solely those of the individual author(s) and contributor(s) and not of MDPI and/or the editor(s). MDPI and/or the editor(s) disclaim responsibility for any injury to people or property resulting from any ideas, methods, instructions or products referred to in the content.